RSC Sustainability

ROYAL SOCIETY OF CHEMISTRY

PAPER

View Article Online
View Journal | View Issue



Cite this: *RSC Sustainability*, 2025, **3**, 2246

# The impact of co-feeding carbon dioxide in Fischer–Tropsch-to-olefin catalysis: an inelastic neutron scattering study

Alisha L. Davidson,[a] Ramandeep S. Dosanjh,[a] Stewart F. Parker [ab] and David Lennon *[a]

Received 19th January 2025
Accepted 14th April 2025

DOI: 10.1039/d5su00042d

rsc.li/rscsus

The addition of $CO_2$ to a syngas feed stream in Fischer–Tropsch to Olefin (FTO) catalysis is investigated by means of inelastic neutron scattering (INS) spectroscopy using ambient pressure CO hydrogenation at 623 K as a test reaction. The principal objective being to explore how the presence of $CO_2$ affects the nature of a hydrocarbonaceous overlayer that forms during the conditioning phase of the catalytic process. The candidate FTO catalyst examined is Fe-based and doubly promoted with sodium (2000 ppm) and sulfur (100 ppm). Temperature-programmed oxidation profiles recorded after 3, 6, 12 and 24 h time-on-stream (T-o-S) reveal progressive carbon retention by the catalyst mainly in the form of amorphous carbon. The INS spectrum as a function of T-o-S confirms the presence of a hydrocarbonaceous overlayer, but with a much higher hydrogen concentration than previously observed for Fe-based FTO catalysts operating solely with a syngas feed. These preliminary results are considered with respect to a possible role for $CO_2$ perturbing the equilibrium between iron carbides and oxides.

**Sustainability spotlight**

Carbon dioxide is a greenhouse gas that is a major contributor to global warming and the climate crisis that the world is presently experiencing. Consequently, there is a major driver to develop chemical manufacturing processes that utilise $CO_2$. The incorporation of $CO_2$ as a feedstock in the emerging Fisher–Tropsch-to-olefins process, a route to produce valuable platform chemicals from biomass, is a candidate process for this role. The article examines fundamental aspects of the surface chemistry of the modified process operation, thereby improving the understanding of how the process could potentially contribute to a global warming mitigation strategy. The article connects with the following 8 UN SDG: 7, 9, 11, 12, 13, 15, 16 and 17.

## 1 Introduction

Fischer–Tropsch synthesis (FTS) over iron-based catalysts is an active area of heterogeneous catalysis research.[1–6] Typically, an oxidic pre-catalyst first undergoes a conditioning process involving the progressive conversion to an iron carbide phase, which is thought to support FTS activity.[7–9] Scheme 1 presents a general overview of this catalyst conditioning process.

Whereas FTS has been extensively investigated by a wide variety of analytical techniques over many years, and despite hydrogen's pivotal role in the catalytic process, uncertainty remains as to how hydrogen is partitioned in the catalyst matrix as a function of reaction conditions. A technique well suited to investigating this conundrum is inelastic neutron scattering (INS), which can provide access to the vibrational spectrum of post-reaction catalyst samples, with special emphasis given to vibrations involving hydrogeneous modes. The topic of using neutron scattering techniques to interrogate heterogeneous catalysts has recently been comprehensively reviewed.[10]

Previous investigations employing inelastic neutron scattering (INS) to study iron-catalysed FTS, using ambient pressure CO hydrogenation as a test reaction, have enabled the vibrational spectrum of the catalyst to be obtained as a function of time-on-stream (T-o-S).[4,5] In addition to the well-documented iron oxide → iron carbide transition (Scheme 1), the INS spectra reveal the additional formation of a hydrocarbonaceous overlayer,[4,5,11–14] which is proposed to perform a 'templating' role in defining the active sites of the working catalyst.[4]

The water gas shift (WGS) reaction (eqn (1)) is also active over iron-based catalysts and is catalyzed by $Fe_3O_4$ that exists in dynamic equilibrium with carbides during FTS.[15–19]

$$CO + H_2O \leftrightharpoons CO_2 + H_2 \quad (1)$$

The WGS reaction is close to equilibrium under high temperature operating conditions and the addition of $CO_2$ to synthesis gas can therefore eliminate its production during FTS,

[a]*School of Chemistry, University of Glasgow, Joseph Black Building, Glasgow, G12 8QQ, UK. E-mail: David.Lennon@glasgow.ac.uk; Tel: +44(0)141 330 4372*

[b]*ISIS Neutron and Muon Facility, STFC Rutherford Appleton Laboratory, Chilton, Didcot, Oxon OX11 0QX, UK*

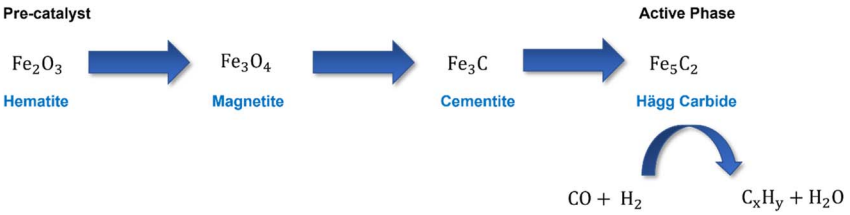


Scheme 1 Overview of how under reaction conditions the hematite pre-catalyst is converted to an iron carbide phase that supports FTS chemistry.



improving carbon efficiency.[20,21] However, as noted by Højlund-Nielsen and Bøgild-Hansen in their pioneering 1982 article, the introduction of $CO_2$ into the feed stream can lead to conversion limitations in hydrocarbon synthesis.[22] Adding further perspective to the role of $CO_2$ in FTS chemistry, in 2021 Claeys and co-workers applied *in situ* magnetometer and X-ray diffraction techniques to investigate how $CO_2$ could perturb reaction equilibria, highlighting the possibility of Hägg carbide oxidation,[7] see Scheme 2. Against a background of increasing concerns over the role of atmospheric $CO_2$ in global warming scenarios, and drivers for nudging chemical manufacturing processes to incorporate $CO_2$ as a reagent (*e.g.* methanol production *via* $CO_2$ hydrogenation),[23] the inclusion of $CO_2$ within a FTS platform represents a tantalising prospect.

In recent times, the formation of long chain saturated hydrocarbons *via* FTS chemistry has been supplemented by a variant known as a Fischer–Tropsch to olefin (FTO) stage. Here, promotion of iron catalysts with an alkali metal and a small concentration of sulfur has been reported to shift the product slate away from long chain saturated hydrocarbons to short chain ($C_2$–$C_4$) olefins, key 'platform chemicals' that find wide application within the chemical industry.[19,24–28] INS studies of FTO catalysts, again using the CO hydrogenation reaction as a test reaction, showed the hydrocarbonaceous overlayer to be similarly formed over the FTO catalysts, although the intensity of the $sp^2$ hybridised C–H stretching mode was amplified relative to an unpromoted hematite sample.[29,30] This modification of the hydrocarbonaceous overlayer was tentatively associated with a reduced hydrogen supply at the catalyst surface that favours olefinicity over saturated products.

Botes and co-workers report on the development of an olefin selective iron Fischer–Tropsch synthesis catalyst and utilise the addition of $CO_2$ in the syngas feed stream during the reaction testing phase of their study.[19] Eqn (1) shows the introduction of $CO_2$ into the syngas feed stream provides an opportunity to increase the CO available for reaction, whilst simultaneously reducing hydrogen availability; a scenario that could minimise C–C chain propagation and the formation of saturated products.

This article seeks to investigate how the addition of $CO_2$ to a $CO/H_2$ feed stream over a representative FTO catalyst, *i.e.* Fe–Na–$S_{100}$,[30,31] can affect the formation of the hydrocarbonaceous overlayer. To this end, ambient pressure CO hydrogenation at 623 K is again selected as the test reaction, as it allows examination of the $Fe/CO/H_2$ surface chemistry without producing high molecular weight hydrocarbon products that would otherwise dominate the INS spectrum.[12] The degree of $CO_2$ incorporation adopted follows that outlined by Botes *et al.*, who utilised a $H_2:CO$ ratio of 4 : 1.[19] Comparisons will be made to previous ambient pressure measurements made at 623 K using the more traditional $H_2:CO = 2:1$ mixture[8] over Fe–Na–$S_{100}$ that are reported elsewhere.[31]

## 2 Experimental

### 2.1. Catalyst preparation

The preparation of Fe–Na–$S_{100}$ utilised a batch reactor that is described elsewhere.[4,14] The preparative method involved the co-precipitation of iron nitrate (Sigma-Aldrich, 99.99%) and sodium carbonate (Sigma-Aldrich, 99.99%), a filtration and washing step followed by the addition of ammonium sulfate (Sigma-Aldrich, 99.99%) and sodium carbonate dissolved in deionised water. The sample was dried, calcined at 623 K for 16 h, then ground and sieved to a particle size range of 250–500 μm.[4,14] The promotional levels of the catalyst were 2000 ppm of Na and 100 ppm of S.[30]

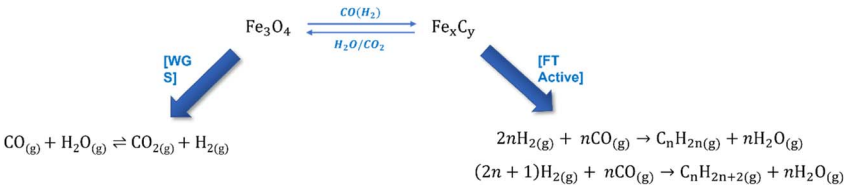


Scheme 2 An illustration indicating how $CO_2$ can work against trends established within the iron-based catalyst conditioning process (Scheme 1), namely inducing the formation of magnetite from iron carbide, with the magnetite supporting WGS chemistry. Figure adapted with permission from M. Claeys, E. van Steen, T. Botha, R. Crous, A. Ferreira, A. Harilal, D. James Moodley, P. Moodley, E. du Plessis and J. L. Visagie, Oxidation of Hägg Carbide during High-Temperature Fischer–Tropsch Synthesis: Size-Dependent Thermodynamics and *In situ* Observations, *ASC Catal.*, 2021, **11**, 13866–13879. Copyright 2021 American Chemical Society.[7]

### 2.2. INS reactor measurements

For INS measurements, approximately 10 g of the promoted catalyst (Fe–Na–$S_{100}$) was loaded into an INS Inconel reactor cell and attached to a custom-built sample preparation rig.[32] A $CO_2$ : CO : $H_2$ feed ratio adopted by Botes and co-workers was used.[19] The sample was heated to 623 K at 5 K $min^{-1}$ under a flow of CO (37.5 sccm), $CO_2$ (25 sccm) $H_2$ (150 sccm) and He (600 sccm), representing a total WHSV of 1.48 $h^{-1}$, and held at temperature (623 K) for varying lengths of time (3, 6, 12 and 24 h).

The product stream was analysed by an in-line mass spectrometer (Hiden Analytical, HPR20 QMS Sampling System). Once the specific reaction was complete, the reactant gases were stopped, and the sample cooled to room temperature under the helium carrier gas. The reactor cell was isolated and placed in an argon-filled glove box (MBraun UniLab MB-20-G, [$H_2O$] < 1 ppm, [$O_2$] < 2 ppm) before the sample was loaded into an aluminium sample holder and sealed *via* an indium wire gasket.[32] All INS measurements were performed using the MAPS direct geometry spectrometer[10] at the ISIS Neutron and Muon Facility (Chilton, UK).[33] Spectra were recorded at 20 K with incident neutron energies of 650 meV and 250 meV using the A-chopper package. Quantification of the $\nu$(C–H) feature observed by INS was achieved following a calibration protocol described elsewhere.[4,5,29–31,34]

*Ex situ* temperature programmed oxidation (TPO) measurements were performed on 10 mg of post-reaction samples using a micro-reactor test line composed of $\frac{1}{8}$ in. diameter stainless steel tubing, a description of which can be found elsewhere.[4,14] The $CO_2$ peak area was quantified by measuring the $CO_2$ response from the *in situ* TPO of known masses of graphite (Sigma-Aldrich, 99.9%).[35] The catalyst was loaded into a $\frac{1}{4}$ in. quartz tube reactor and plugged with quartz wool. The reactor was housed within a tube furnace (Carbolite MTF 10/15/30) equipped with PID control. All gas flows were monitored using an in-line quadruple mass spectrometer (Hiden Analytical, HPR-20) attached to the reactor exit line *via* a differentially pumped, heated quartz capillary. Oxygen (5% in He, 75 sccm, BOC Ltd, 99.5%) was introduced to the sample and the reactor heated to 1173 K at 5 K $min^{-1}$ using the mass spectrometer to monitor the eluting gases.

## 3 Results and discussion

### 3.1. Reaction testing and characterisation

Fe–Na–$S_{100}$ has been utilised in previous FTO investigations and characterisation of this material is reported elsewhere.[30]

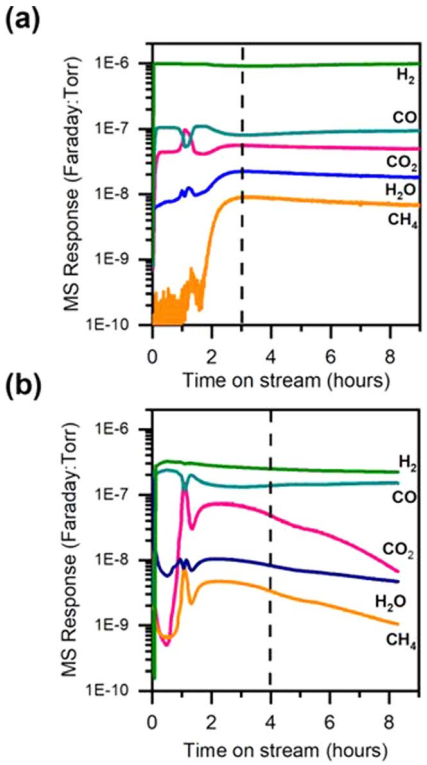


Fig. 1 Reaction profile of Fe–Na–$S_{100}$ exposed to (a) ambient pressure CO hydrogenation at 623 K with a $CO_2$ co-feed (6 : 1.5 : 1 $H_2$ : CO : $CO_2$) (b) ambient pressure CO hydrogenation at 623 K without a $CO_2$ co-feed (2 : 1 $H_2$ : CO). Both measurements correspond to the INS Inconel reactor.

Aspects of that study included reaction testing under representative FT conditions of elevated temperature and pressure. Table 1 presents information on the product slate of the Fe–Na–$S_{100}$ catalyst alongside that of an unpromoted Fe catalyst that represents a reference standard. Table 1 shows the promoted catalyst to exhibit significantly enhanced olefin : paraffin ratios for $C_2$, $C_3$ and $C_4$ moieties.

In this study, Fe–Na–$S_{100}$ was exposed to ambient pressure CO hydrogenation conditions at 623 K with the inclusion of a $CO_2$ co-feed, for 3, 6, 12 and 24 h, with a representative profile shown in Fig. 1a. This is directly compared in Fig. 1b to the same catalyst, Fe–Na–$S_{100}$, exposed to ambient-pressure CO hydrogenation conditions without a $CO_2$ feed in the same reactor, as reported in a previous study.[31] Whereas previous

Table 1 Selectivity data of an unpromoted Fe catalyst [Fe-ref] and the Fe–Na (2000 ppm)–S (100 ppm) catalyst [Fe–Na–$S_{100}$] exposed to FTS conditions (20 bar, 4 : 1 $H_2$ : CO, $T$ = 603 K) for 6 h T-o-S. The $C_2$–$C_4$ and $C_{5+}$ classifications correspond to saturated and unsaturated products. FT activity is based on CO conversion that excludes CO → $CO_2$ production. The errors correspond to variation in the individual measurements as determined from a series of repeat measurements over a standard (unspecified) reference catalyst. The table is adapted from ref. 30 with permission

| Sample | FT [μmol $g^{-1}$ $s^{-1}$] | $CH_4$ (%) | $CO_2$ (%) | $C_2$–$C_4$ (%) | $C_{5+}$ (%) | $C_2$ olefin : paraffin | $C_3$ olefin : paraffin | $C_4$ olefin : paraffin |
|---|---|---|---|---|---|---|---|---|
| Fe-ref | 78.5 ± 3.9 | 24.9 ± 1.2 | 26.2 ± 1.3 | 41.8 ± 2.1 | 33.3 ± 1.7 | 0.1 ± 0.01 | 0.8 ± 0.04 | 1.3 ± 0.1 |
| Fe–Na–$S_{100}$ | 47.9 ± 2.4 | 9 ± 0.5 | 33.6 ± 1.7 | 34.2 ± 1.7 | 56.8 ± 2.8 | 8.1 ± 0.4 | 8.7 ± 0.5 | 7.8 ± 0.4 |

studies using a micro-reactor arrangement revealed a three-stage conditioning process that involved the transitions indicated in Scheme 1,[4,5,14] Fig. 1 is better described by a two-stage process: the initial reduction step requires approximately 2 h T-o-S; thereafter, the system exhibits pseudo-steady state operation. This scenario applies both to Fig. 1a and b. It is possible that the larger Inconel reactor is causing a reduction in profile resolution compared to the micro-reactor studies.

Fig. 1a shows the inclusion of $CO_2$ into the feedstream leads to more stable methane production on completion of the reduction stage compared to its absence (Fig. 1b). The water production is also more stable. Thus, the $CO_2$ appears to have induced changes to the reaction profile but only to a modest degree. No $C_2$–$C_4$ olefins or higher hydrocarbons were observed for these ambient pressure measurements conducted in the INS Inconel reactor. As noted in the Introduction, the reaction conditions used by Botes *et al.*[19] means that the hydrogen ratio used in the two runs presented in Fig. 1 is higher for the $CO_2$ co-feed case, a situation that potentially compromises direct comparisons between the two runs.

Fig. 2 presents the *ex situ* post-reaction temperature-programmed oxidation (TPO) profiles after 3, 6, 12 and 24 h of reaction, showing $CO_2$ production that signifies carbon retention by the catalyst. Fig. 3 displays the oxygen consumption profiles alongside the individual TPO plots, confirming that the provision of the oxidant was sufficient in all cases. Previous studies have identified and quantified three distinct carbonaceous components: α – reactive carbon, β – amorphous carbon and γ – iron carbides/polyaromatic carbonaceous species.[4,5,30,31] Fig. 4 compares the TPO profiles for the Fe–Na–$S_{100}$ catalyst after 12 h reaction (ambient pressure CO hydrogenation at 623 K) in the absence (red) and presence (blue) of a $CO_2$ co-feed. Whilst the α, β and γ features are observable when $CO_2$ is absent, peak resolution is degraded when $CO_2$ is present, and the profile is dominated by an intense feature exhibiting a peak maximum in the range 650–680 K. On the basis of the $T_{max}$ value, the desorption feature is assigned to amorphous carbon.[31] It is surmised that the larger amounts of carbon laydown observed in the presence of the $CO_2$ co-feed (Fig. 4) are responsible for the lower resolution TPO profiles.

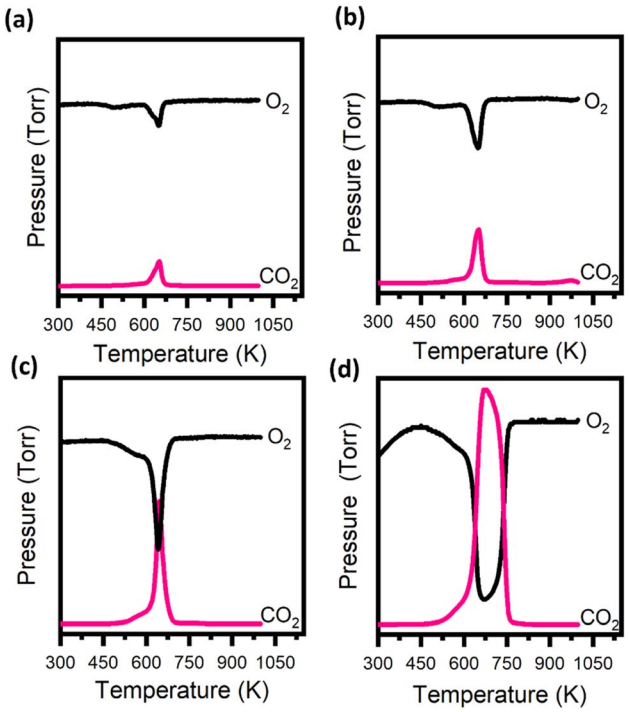


Fig. 3 TPO profiles (pink) for T-o-S = (a) 3, (b) 6, (c) 12 and (d) 24 h, with the figures including the associated oxygen consumption profiles (black).

Fig. 5 correlates the extent of total carbon retention as a function of T-o-S for reactions undertaken in the presence of $CO_2$. The total quantity of carbon retention after 24 h T-o-S is 430 $mmol_C\ g_{Fe}^{-1}$. This value significantly exceeds that reported for an unpromoted hematite Fischer–Tropsch synthesis catalyst operating solely with a 2 : 1 syngas feed (24 h T-o-S = 27 $mmol_C\ g_{Fe}^{-1}$)[31] by a factor of >16. Moreover, the overall profile can be

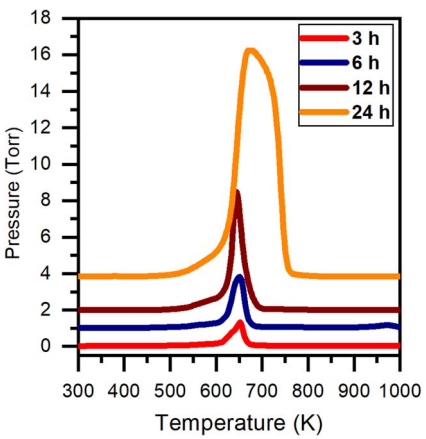


Fig. 2 *Ex situ* temperature-programmed oxidation profiles for Fe–Na–$S_{100}$ after exposure to CO hydrogenation conditions with a $CO_2$ co-feed at 623 K for 3, 6, 12 and 24 h T-o-S.

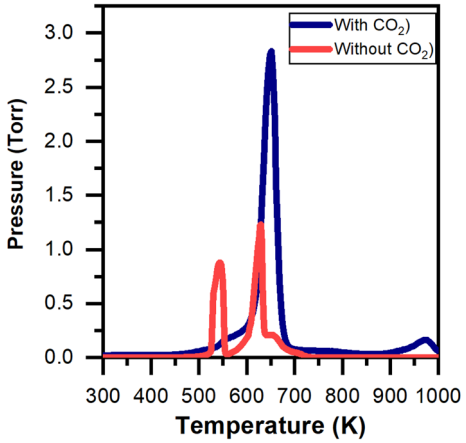


Fig. 4 *Ex situ* temperature-programmed oxidation profiles for Fe–Na–$S_{100}$ after exposure to CO hydrogenation conditions with (blue) and without (red) a $CO_2$ co-feed at 623 K for 24 h T-o-S. The 'without $CO_2$' profile has been reported previously by Davidson *et al.*[31] and is included in this figure for comparison purposes.

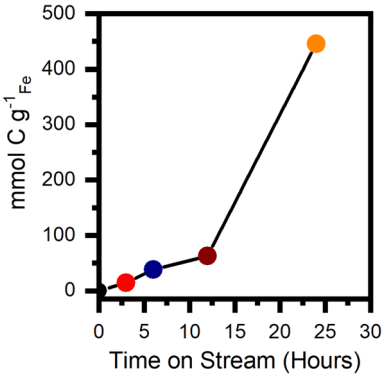


Fig. 5 (a) Carbon content ($mmol_C\ g_{Fe}^{-1}$) observed from the *ex situ* TPO profiles of samples exposed to CO hydrogenation conditions with a $CO_2$ co-feed for 3, 6, 12 and 24 h.

deconvoluted into two kinetic regimes: the period 0–12 h T-o-S corresponds to a carbon deposition rate of 5.0 $mmol_C\ g_{Fe}^{-1}\ h^{-1}$, whilst the period 12–24 h corresponds to a retention rate of 32.5 $mmol_C\ g_{Fe}^{-1}\ h^{-1}$, *i.e.* 6.5 times that observed for the lower runtimes.

Lastly for this section, it is noted that on transferring the 24 h reacted sample from the large-scale Inconel reactor to the aluminium INS sample holder in the glove box, large quantities of carbon were clearly observed. The visual extent of this carbon formation exceeded anything previously seen for this campaign of INS investigations of FTS and FTO catalysis.[4,5,11–14,29–32]

### 3.2. INS measurements

Fig. 6 presents the INS spectra for the Fe–Na–$S_{100}$ catalyst recorded at incident energies of 650 and 250 meV. The left-hand frames show the spectra for reactions performed where $CO_2$ is included in the feedstream, with spectra recorded after runtimes of 3, 6, 12 and 24 h (red, blue, brown and orange plots). For comparison, the right-hand frames present the spectra for the Fe–Na–$S_{100}$ catalyst after 24 h reaction at 623 K in the absence of $CO_2$ (green plots).

For the $CO_2$ included dataset, inspection of the stretching region (2400–3750 $cm^{-1}$) presented in Fig. 6a identifies the presence of hydrocarbon moieties, with a prominent $sp^2$ hybridised carbon $\nu$(C–H) feature at 3048 $cm^{-1}$ and a $sp^3$ hybridised carbon $\nu$(C–H) shoulder at 2932 $cm^{-1}$ observed for

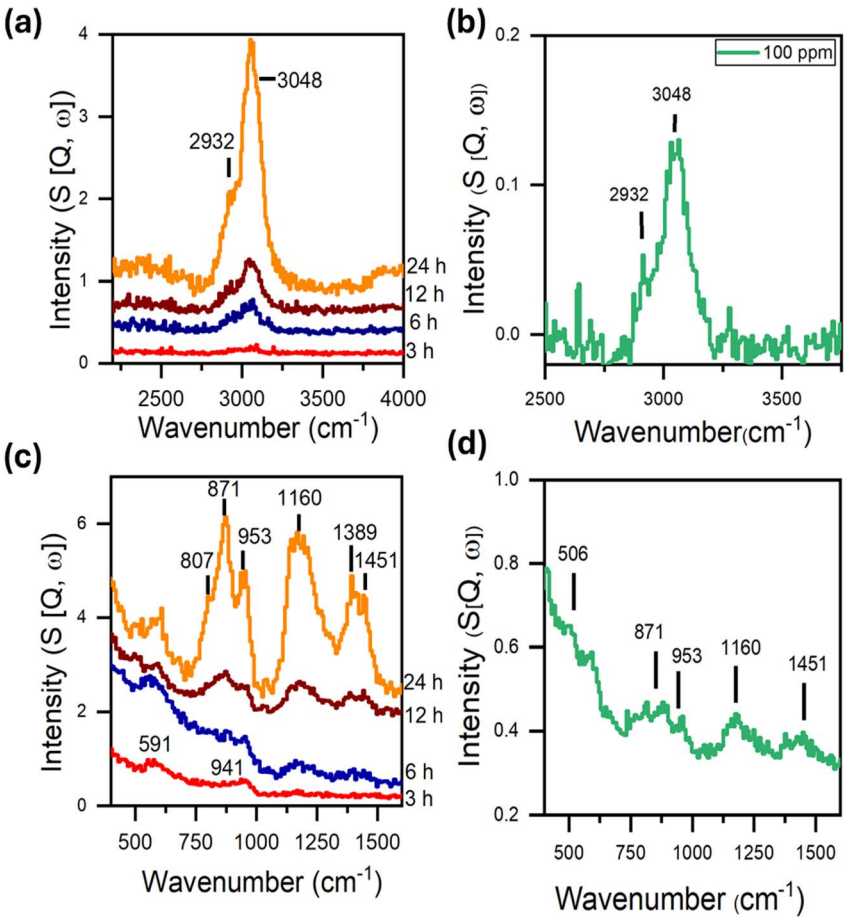


Fig. 6 The left-hand frames present INS spectra for the Fe-based doubly promoted Fischer–Tropsch catalyst (Fe–Na–$S_{100}$) after CO hydrogenation with a $CO_2$ co-feed at 623 K for 0–24 h (red, blue, brown and orange) with incident energies of (a) 650 meV and (c) 250 meV. The right-hand frames present INS spectra for the Fe-based doubly promoted Fischer–Tropsch catalyst (Fe–Na–$S_{100}$) after CO hydrogenation performed in the absence of a $CO_2$ co-feed at 623 K for 24 h (green) with incident energies of (b) 650 meV and (d) 250 meV. The spectra presented in (b) and (d) have been reported previously by Davidson *et al.*[31] and are included in this figure for comparison purposes.

all samples.[4,29–31] The deformation region of the spectra (400–1600 $cm^{-1}$) (Fig. 6c), highlights various bands that have been observed previously.[4,5,11–13,29–32] These can be summarised as follows: C–C torsion mode of edge carbon atoms contained within a polycyclic aromatic network (506 $cm^{-1}$); out-of-plane C–H deformation of either an olefinic or aromatic group (871 $cm^{-1}$); alkenic $\delta$(C–H) (953 $cm^{-1}$); CC–H in plane deformation of a polyaromatic hydrocarbon (1160 $cm^{-1}$) and methyl deformation modes (1389, 1451 $cm^{-1}$).[30] Overall, with the inclusion of the $CO_2$ co-feed, the INS spectrum for the FTO catalyst by 24 h T-o-S (Fig. 6a and c) is comparable to that previously reported for Fe–Na–$S_{100}$ under standard CO hydrogenation conditions (Fig. 6b and d).[31] This coincidence in the overall spectral profile signifies that, despite the alteration to the feed stream, the nature of the hydrocarbonaceous overlayer is effectively unchanged.

However, other aspects of the INS spectrum are noticeably different. Specifically, for Fe–Na–$S_{100}$ in the absence of $CO_2$ it is reported that a band at 591 $cm^{-1}$, assigned to the $A_{1g}$ phonon of magnetite ($Fe_3O_4$) and indicative of an under reduced catalyst, is only prominently observable up to 3 h on stream.[31] Notably, this band is only weakly observed in Fig. 6d. In contrast, Fig. 6c shows this feature to be retained throughout the full 24 h period. Following the lead of Højund-Nielsen and Bøgild-Hansen,[22] and with reference to the equilibrium condition depicted in Scheme 2, a possible explanation is that the presence of $CO_2$ prevents complete reduction of magnetite to Hägg carbide; either at the surface, in the bulk, or indeed both. This effect of $CO_2$ co-feeding has also been observed recently in similar studies of fused iron catalysts.[16]

On employing previously established calibration procedures,[4,5,10–14,29–31] the hydrogen concentration of the $\nu$(C–H) modes observed in Fig. 6a can be quantified and are presented in Fig. 7. Both the aliphatic (2932 $cm^{-1}$) and aromatic/olefinic (3048 $cm^{-1}$) components of the hydrocarbonaceous overlayer in the presence of $CO_2$ show comparable profiles, increasing steadily to 12 h on stream before exhibiting a dramatic change in formation rate. For the period 0–12 h T-o-S the $sp^2$ hybridised carbon $\nu$(C–H) feature at 3048 $cm^{-1}$ signifies a formation rate of 2.3 $\mu mol_H\ g_{Fe}^{-1}\ h^{-1}$, whilst for the period 12–24 h this rises to a value of 7.4 $\mu mol_H\ g_{Fe}^{-1}\ h^{-1}$, corresponding to an increase of $\times$ 3.2. At T-o-S = 24 h, the $sp^3$ and $sp^2$ hybridised $\nu$(C–H) components respectively correspond to 23 and 116 $\mu mol_H\ g_{Fe}^{-1}$. This sudden increase in INS intensity, signifying an increase in retained hydrogen, is unprecedented. For example, Fig. 7 additionally presents the hydrogen retention values for the $sp^3$ and $sp^2$ hybridised $\nu$(C–H) components of Fe–Na–$S_{100}$ determined in the absence of a $CO_2$ co-feed (dashed lines).[31] These values (3.7 and 9.6 $\mu mol_H\ g_{Fe}^{-1}$ respectively) are an order of magnitude below that seen in the presence of the $CO_2$ co-feed.

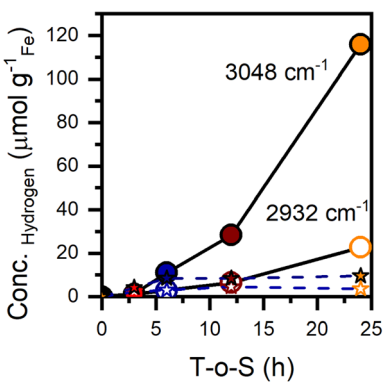


Fig. 7 Hydrogen concentration ($\mu mol\ g_{Fe}^{-1}$) of $sp^3$ hybridised carbon feature at 2932 $cm^{-1}$ (hollow) and $sp^2$ hybridised carbon feature at 3048 $cm^{-1}$ (solid) identified in Fig. 6(a) of Fe–Na–$S_{100}$ in the presence of $CO_2$ (solid lines), and in the absence of $CO_2$ (dashed lines).

## 4 Discussion

The inclusion of $CO_2$ clearly perturbs the FTO chemistry. When $CO_2$ is added to a syngas feedstream over Fe–Na–$S_{100}$ the TPO measurements show excessive formation of amorphous carbon (Fig. 2, 4 and 5), whilst after 24 h T-o-S INS also reveals an order of magnitude increase in the intensity of $\nu$(C–H) modes associated with the presence of a hydrocarbonaceous overlayer (Fig. 7). Moreover, the INS band at 591 $cm^{-1}$ indicates the presence of magnetite. Following on from Højund-Nielsen and Bøgild-Hansen,[22] Claeys and co-workers use the following two equations to describe how the oxidising agents $H_2O$ and/or $CO_2$ could induce the conversion of FT active Hägg carbide to magnetite.[7]

$$3Fe_5C_2 + 26H_2O \rightarrow 5Fe_3O_4 + 6CO + 26H_2 \quad (2)$$

$$3Fe_5C_2 + 26CO_2 \rightarrow 5Fe_3O_4 + 32CO \quad (3)$$

Fig. 1 indicates continuous CO and $H_2$ turnover that is maintained with the addition of $CO_2$ to the syngas feedstream. The observation of magnetite in the INS spectra is attributed to the presence of $CO_2$ retarding bulk carbide formation during activation rather than preventing complete surface reduction or causing re-oxidation at the onset of catalyst turnover.

The temporal profiles of the TPO plots and the INS intensities hint at coordinated events occurring at the catalyst surface. Concentrating firstly on the carbon, Fig. 5 shows the formation of amorphous carbon signal to dramatically increases at T-o-S = 12 h. Specifically, a 6.5-fold increase in the carbon deposition rate is observed for the period 12–24 h compared to that consistently observed in the first 12 h period. Poignantly, Fig. 7 shows this reaction time coincides with a significant increase in the concentration of the hydrocarbonaceous overlayer, as signified by the intensity of the $sp^2$ hybridised carbon $\nu$(C–H) feature at 3048 $cm^{-1}$, which exhibits a 3.2-fold increase for the latter 12 h period of T-o-S compared to that observed during the initial 12 h block. Within the complexity of the iron catalyst's conditioning phase (Scheme 1), we propose that the level of $CO_2$ inclusion and operating conditions used here can progressively modify the chemical potential of the surface. The precise way this occurs is uncertain. Indeed, in a way, the TPO and INS trends are contradictory: the extensive carbon formation hints at hydrogen-lean conditions (which would favour olefin formation), whilst the enhanced incorporation of hydrogen into

the hydrocarbonaceous overlayer seemingly goes against this trend.

The relative rates of enhancement observed for periods exceeding 12 h T-o-S are informative concerning a possible inter-play between carbon retention and a hydrocarbonaceous overlayer. In their examination of the temporal behaviour of an unpromoted FTS catalyst applied to ambient pressure CO hydrogenation at 623 K, Warringham and co-workers proposed a reaction model where amorphous carbon formation and a hydrocarbonaceous overlayer were individual components of a conditioned catalyst.[14] Whilst a consideration of a synchronised increase in the rate of amorphous carbon build-up and enhanced formation of the $sp^2$ hybridised carbon $\nu$(C–H) mode, as signified in, respectively, Fig. 5 and 7, may suggest that the carbon and hydrogen retention processes are inherently linked, inspection of their relative formation rates suggests otherwise. Rather, it is thought that following a catalyst conditioning stage of 12 h duration, the greater acceleration of carbon retention over that of generation of hydrocarbonaceous species (carbon accumulation is approximately twice that of hydrogen retention) is indicative of distinct processes taking place, as invoked within Warringham and co-workers' reaction model.[14] Concerning the substantial quantities of amorphous carbon being produced, this could be due to the Boudouard reaction (eqn (4)).

$$2CO \leftrightharpoons CO_2 + C \quad (4)$$

Whereas this study has adopted the $H_2$ : CO ratio of 4 : 1 v/v as outlined by Botes and co-workers,[19] so that possible advantages connected with eqn (1) can be assessed, this has meant that comparisons to previous measurements over the Fe–Na–$S_{100}$ catalyst performed using a $H_2$ : CO ratio of 2 : 1 v/v, as commonly encountered in FTS chemistry,[8] are non-ideal. As ever with Fe-based FTS and FTO catalysts, the water gas shift reaction adds further complexity over and above that encountered with the already complex syngas/Fe interactions. Nonetheless, given the potential of FTO chemistry to produce valuable 'platform' chemicals from a variety of carbon sources, including biomass, and an inherent driver to adapt large-scale chemical process operations to utilise $CO_2$, the complexity of events active within this commercially relevant reaction system, as highlighted in this study, is deemed to be worthy of further investigation.[36] This could include an assessment of the sensitivity of reaction performance to $CO_2$ concentration in the feed gas.

# 5 Conclusions

Ambient pressure CO hydrogenation with a $CO_2$ co-feed over a doubly promoted FTO catalyst (Fe–Na–$S_{100}$) at 623 K has been investigated over a 24 h period and characterised post-reaction by TPO and INS. The following conclusions can be drawn.

• In comparison to operation in the absence of $CO_2$, the reaction profile exhibits increased and sustained methane production (Fig. 1).

• The presence of $CO_2$ leads to a substantial increase in the formation of amorphous carbon. After 24 h T-o-S this corresponds to 430 $mmol_C\ g_{Fe}^{-1}$ (Fig. 5), a value 16 times greater than that observed in the absence of $CO_2$.

• The presence of $CO_2$ in the syngas feedstream appears to have no significant effect on the form of a hydrocarbonaceous overlayer, the spectra exhibiting a comparable spectral profile to that observed for FTS and FTO catalysts (Fig. 6).

• The degree of hydrogen incorporation within the hydrocarbonaceous overlayer is considerably increased in the presence of a $CO_2$ co-feed (Fig. 7). For example, after 24 h T-o-S the $sp^2$ hybridised $\nu$(C–H) component corresponds to 116 $\mu mol_H\ g_{Fe}^{-1}$, compared to a value of 9.6 $\mu mol_H\ g_{Fe}^{-1}$ in the absence of $CO_2$, a 12-fold enhancement.

• A coincidence of increased rates of carbon (Fig. 5) and hydrogen (Fig. 7) retention into the catalyst matrix is observed at 12 h T-o-S. Given the approximately two-fold disparity in retention rate enhancement for carbon compared to hydrogen, these are thought to represent distinct chemical pathways.

# Data availability

The data that support the findings of this study, including spectroscopic datasets, are available *via* the University of Glasgow Library [DOI: **https://doi.org/10.5525/gla.researchdata.1872**].

# Author contributions

Alisha L. Davidson: methodology, validation, formal analysis, investigation, data curation, writing – original draft, writing – review & editing, supervision. Ramandeep S. Dosanjh: investigation, writing – review & editing. Stewart F. Parker: methodology, validation, investigation, writing – review & editing, supervision. David Lennon: conceptualization, methodology, formal analysis, resources, writing – review & editing, supervision, project administration, funding acquisition.

# Conflicts of interest

There are no conflicts to declare.

# Acknowledgements

Dr Paul Webb (University of St. Andrews) is thanked for project support and guidance. Sasol Ltd., the University of Glasgow and the EPSRC [award reference EP/P505534/1] are thanked for the provision of a postgraduate studentship (ALD). The STFC Rutherford Appleton Laboratory is thanked for access to neutron beam facilities *via* RB1820113.36.

# References

1 J. Van de Loosdrecht, F. G. Botes, I. M. Ciobica, A. C. Ferreira, P. Gibson, D. J. Moodley, A. M. Saib, J. L. Visagie, C. J. Weststrate and J. W. Niemantsverdriet, in *Comprehensive Inorganic Chemistry II : from elements to applications*, ed. J. Reedijk and K. Poeppelmeier, Elsevier, 2013, pp. 525–557.

2 H. Ando, Y. Matsumura and Y. Souma, A comparative study on hydrogenation of carbon dioxide and carbon monoxide over iron catalyst, *J. Mol. Catal. A: Chem.*, 2000, **154**, 23–29.
3 O. O. James, B. Chowdhury, M. A. Mesubi and S. Maity, Reflections on the chemistry of the Fischer–Tropsch synthesis, *RSC Adv.*, 2012, **2**, 7347.
4 R. Warringham, A. L. Davidson, P. B. Webb, R. P. Tooze, R. A. Ewings, S. F. Parker and D. Lennon, Examining the temporal behavior of the hydrocarbonaceous overlayer on an iron based Fischer–Tropsch catalyst, *RSC Adv.*, 2019, **9**, 2608–2617.
5 A. L. Davidson, P. B. Webb, S. F. Parker and D. Lennon, Hydrogen Partitioning as a Function of Time-on-Stream for an Unpromoted Iron-Based Fischer–Tropsch Synthesis Catalyst Applied to CO Hydrogenation, *Ind. Eng. Chem. Res.*, 2020, **59**, 52–60.
6 M. Amin, M. Usman, T. Kella, W. U. Khan, I. A. Khan and K. Hoon Lee, Issues and challenges of Fischer–Tropsch synthesis catalysts, *Front. Chem.*, 2024, **12**, 1462503.
7 M. Claeys, E. van Steen, T. Botha, R. Crous, A. Ferreira, A. Harilal, D. James Moodley, P. Moodley, E. du Plessis and J. L. Visagie, Oxidation of Hägg Carbide during High-Temperature Fischer–Tropsch Synthesis: Size-Dependent Thermodynamics and *In Situ* Observations, *ASC Catal.*, 2021, **11**, 13866–13879.
8 T. Herranz, S. Rojas, F. Perezalonso, M. Ojeda, P. Terreros and J. Fierro, Genesis of iron carbides and their role in the synthesis of hydrocarbons from synthesis gas, *J. Catal.*, 2006, **243**, 199–211.
9 P. P. Paalanen, S. H. van Vreeswijk and B. M. Weckhuysen, Combined *In Situ* X-ray Powder Diffractometry/Raman Spectroscopy of Iron Carbide and Carbon Species Evolution in Fe(−Na–S)/α-$Al_2$ $O_3$ Catalysts during Fischer–Tropsch Synthesis, *ACS Catal.*, 2020, **10**, 9837–9855.
10 S. F. Parker, D. Lennon and P. W. Albers, Vibrational Spectroscopy with Neutrons: A Review of New Directions, *Appl. Spectrosc.*, 2011, **65**, 1325–1341.
11 N. G. Hamilton, I. P. Silverwood, R. Warringham, J. Kapitán, L. Hecht, P. B. Webb, R. P. Tooze, S. F. Parker and D. Lennon, Vibrational Analysis of an Industrial Fe-Based Fischer–Tropsch Catalyst Employing Inelastic Neutron Scattering, *Angew. Chem., Int. Ed.*, 2013, **52**, 5608–5611.
12 N. G. Hamilton, R. Warringham, I. P. Silverwood, J. Kapitán, L. Hecht, P. B. Webb, R. P. Tooze, W. Zhou, C. D. Frost, S. F. Parker and D. Lennon, The application of inelastic neutron scattering to investigate CO hydrogenation over an iron Fischer–Tropsch synthesis catalyst, *J. Catal.*, 2014, **312**, 221–231.
13 R. Warringham, N. G. Hamilton, I. P. Silverwood, C. How, P. B. Webb, R. P. Tooze, W. Zhou, C. D. Frost, S. F. Parker and D. Lennon, The application of inelastic neutron scattering to investigate a hydrogen pre-treatment stage of an iron Fischer–Tropsch catalyst, *Appl. Catal., A*, 2015, **489**, 209–217.
14 R. Warringham, A. R. McFarlane, D. A. MacLaren, P. B. Webb, R. P. Tooze, J. Taylor, R. A. Ewings, S. F. Parker and D. Lennon, The application of inelastic neutron scattering to explore the significance of a magnetic transition in an iron based Fischer–Tropsch catalyst that is active for the hydrogenation of CO, *J. Chem. Phys.*, 2015, **143**, 174703.
15 D. S. Newsome, The Water-Gas Shift Reaction, *Catal. Rev.*, 1980, **21**, 275–318.
16 H. Zhang, Characterization of a fused iron catalyst for Fischer–Tropsch synthesis by *in situ* laser Raman spectroscopy, *J. Catal.*, 1985, **95**, 325–332.
17 E. S. Lox and G. F. Froment, Kinetics of the Fischer–Tropsch reaction on a precipitated promoted iron catalyst. 1. Experimental procedure and results, *Ind. Eng. Chem. Res.*, 1993, **32**, 61–70.
18 D. G. Rethwisch and J. A. Dumesic, Adsorptive and Catalytic Properties of Supported Metal Oxides, *J. Catal.*, 1986, **101**, 35–42.
19 G. F. Botes, T. C. Bromfield, R. L. J. Coetzer, R. Crous, P. Gibson and A. C. Ferreira, Development of a chemical selective iron Fischer–Tropsch catalyst, *Catal. Today*, 2016, **275**, 40–48.
20 S. Li, S. Krishnamoorthy, A. Li, G. D. Meitzner and E. Iglesia, Promoted Iron-Based Catalysts for the Fischer–Tropsch Synthesis: Design, Synthesis, Site Densities, and Catalytic Properties, *J. Catal.*, 2002, **206**, 202–217.
21 S. Krishnamoorthy, A. Li and E. Iglesia, Pathways for CO2 Formation and Conversion During Fischer–Tropsch Synthesis on Iron-Based Catalysts, *Catal. Lett.*, 2002, **80**, 77–86.
22 P. E. Højlund-Nielsen and J. Bøgild-Hansen, Conversion limitations in hydrocarbon synthesis, *J. Mol. Catal.*, 1982, **17**, 183–193.
23 M. Bowker, N. Lawes, I. Gow, J. Hayward, J. R. Esquius, N. Richards, L. R. Smith, T. J. A. Slater, T. E. Davies, N. F. Dummer, L. Kabalan, A. Logsdail, R. C. Catlow, S. Taylor and G. J. Hutchings, The Critical Role of βPdZn Alloy in Pd/ZnO Catalysts for the Hydrogenation of Carbon Dioxide to Methanol, *ACS Catal.*, 2022, **12**, 5371–5379.
24 P. P. Paalanen and B. M. Weckhuysen, Carbon Pathways, Sodium-Sulphur Promotion and Identification of Iron Carbides in Iron-based Fischer–Tropsch Synthesis, *ChemCatChem*, 2020, **12**, 4202–4223.
25 T. C. Bromfield and N. J. Coville, The effect of sulfide ions on a precipitated iron Fischer–Tropsch catalyst, *Appl. Catal., A*, 1999, **186**, 297–307.
26 A. J. McCue and J. A. Anderson, Sulfur as a catalyst promoter or selectivity modifier in heterogeneous catalysis, *Catal. Sci. Technol.*, 2014, **4**, 272–294.
27 H. M. Torres Galvis and K. P. de Jong, Catalysts for Production of Lower Olefins from Synthesis Gas: A Review, *ACS Catal.*, 2013, **3**, 2130–2149.
28 P. B. Webb and I. A. W. Filot, in *Comprehensive Inorganic Chemistry III*, Elsevier, 2023, pp. 354–380.
29 R. Warringham, A. L. Davidson, P. B. Webb, R. P. Tooze, S. F. Parker and D. Lennon, Perspectives on the effect of sulfur on the hydrocarbonaceous overlayer on iron Fischer–Tropsch catalysts, *Catal. Today*, 2020, **339**, 32–39.

30 A. L. Davidson, E. K. Gibson, G. Cibin, H. Van Rensburg, S. F. Parker, P. B. Webb and D. Lennon, The application of inelastic neutron scattering to investigate iron-based Fischer–Tropsch to olefins catalysis, *J. Catal.*, 2020, **392**, 197–208.

31 A. L. Davidson, P. B. Webb, S. F. Parker and D. Lennon, An Inelastic Neutron Scattering Investigation of the Temporal Behaviour of the Hydrocarbonaceous Overlayer of a Prototype Fischer–Tropsch to Olefins Catalyst, *Top. Catal.*, 2021, **64**, 631–637.

32 R. Warringham, D. Bellaire, S. F. Parker, J. Taylor, R. A. Ewings, C. M. Goodway, M. Kibble, S. R. Wakefield, M. Jura, M. P. Dudman, R. P. Tooze, P. B. Webb and D. Lennon, Sample environment issues relevant to the acquisition of inelastic neutron scattering measurements of heterogeneous catalyst samples, *J. Phys.: Conf. Ser.*, 2014, **554**, 012005.

33 ISIS Neutron and Muon Source:hma About, **https://www.isis.stfc.ac.uk/Pages/About.aspx**, accessed 3 January 2025.

34 I. P. Silverwood, N. G. Hamilton, C. J. Laycock, J. Z. Staniforth, R. M. Ormerod, C. D. Frost, S. F. Parker and D. Lennon, Quantification of surface species present on a nickel/alumina methane reforming catalyst, *Phys. Chem. Chem. Phys.*, 2010, **12**, 3102.

35 I. P. Silverwood, N. G. Hamilton, A. R. McFarlane, J. Kapitán, L. Hecht, E. L. Norris, R. M. Ormerod, C. D. Frost, S. F. Parker and D. Lennon, Application of inelastic neutron scattering to studies of $CO_2$ reforming of methane over alumina-supported nickel and gold-doped nickel catalysts, *Phys. Chem. Chem. Phys.*, 2012, **14**, 15214–15225.

36 D. Lennon, A. L. Davidson, S. F. Parker, P. B. Webb, *The application of INS to examine a Fischer–Tropsch-to-olefin catalyst that has been reacted in the presence of $CO_2$*, STFC ISIS Neutron and Muon Source, 2018, DOI: **10.5286/ISIS.E.1820113**.